NANO LETTERS
Cite This: Nano Lett. XXXX, XXX, XXX−XXX
Letter
pubs.acs.org/NanoLett

Ultranarrow Second-Harmonic Resonances in Hybrid Plasmon-Fiber Cavities

Qi Ai,[*,†] Lili Gui,[*,†] Domenico Paone,[†] Bernd Metzger,[†] Martin Mayer,[‡,§] Ksenia Weber,[†] Andreas Fery,[‡,§,∥] and Harald Giessen[*,†]

[†]4th Physics Institute and Research Center SCoPE, University of Stuttgart, Pfaffenwaldring 57, 70569 Stuttgart, Germany
[‡]Institute of Physical Chemistry and Polymer Physics, Leibniz-Institut für Polymer Forschung Dresden e.V. (IPF), Hohe Strasse 6, 01069 Dresden Germany
[§]Cluster of Excellence Center for Advancing Electronics Dresden (cfaed) and [∥]Physical Chemistry of Polymeric Materials, Technische Universität Dresden, 01062 Dresden, Germany

S *Supporting Information*

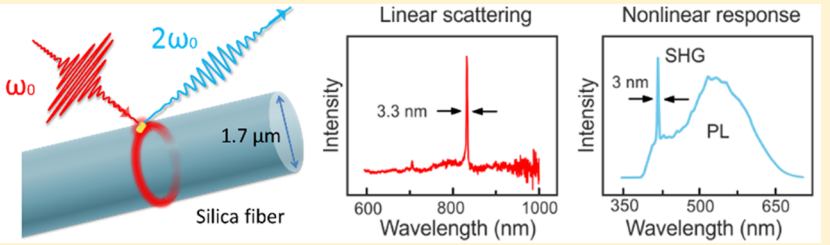

ABSTRACT: We demonstrate second-harmonic generation with ultranarrow resonances in hybrid plasmon-fiber cavities, formed by depositing single-crystalline gold nanorods onto the surface of tapered microfibers with diameters in the range of 1.7−1.8 μm. The localized surface plasmon mode of the single gold nanorod efficiently couples with a whispering gallery mode of the fiber, resulting in a very narrow hybrid plasmon-fiber resonance with a high quality factor Q of up to 250. When illuminated with a tunable 100 fs laser, a sharp SHG peak narrower than half of the spectral width of the impinging laser emerges, superimposed on a broad multiphoton photoluminescence background. The enhancement of the SHG peak of the hybrid system is typically 1000-fold when compared to that of a single gold nanorod alone. Tuning the laser over the hybrid resonance enables second-harmonic spectroscopy and yields an ultranarrow line width as small as 6.4 nm. We determine the second-harmonic signal to rise with the square of the laser power, while the multiphoton photoluminescence background rises with powers between 4 and 6, indicating a very efficient higher-order process. A coupled anharmonic oscillator model is able to describe the linear as well as second-harmonic resonances very well. Our work will open the door to the simultaneous utilization of narrow whispering gallery resonances together with high plasmonic near-field enhancement and should allow for nonlinear sensing and extremely efficient nonlinear light generation from ultrasmall volumes.

KEYWORDS: *Nonlinear plasmonics, narrow linewidth, second-harmonic generation, nanooptics, whispering gallery mode, gold nanorods*

Gaining from very high optical nonlinearities of noble metals together with significantly enhanced optical near-fields, nonlinear plasmonics has attracted a lot of attention in the past years. Experiments with femtosecond lasers and resonant plasmonic systems yielded efficient nonlinear effects such as second- and third-harmonic generation (SHG and THG),[1−7] four-wave mixing,[8,9] ultrafast optical switching,[10,11] and multiphoton photoluminescence (MPPL)[12−16] from very small volumes beyond the diffraction limit, opening the door for nonlinear photonic devices on the nanometer scale.

Until now, the power of the generated nonlinear light in nanostructures is still very weak. Several approaches have been pursued in order to promote the conversion efficiency. One prominent way is to combine other highly nonlinear materials such as semiconductors,[17,18] polymers,[19,20] dielectrics,[21] and so forth, in which the plasmonic structures are usually resonant at the excitation wavelength. Another method is using multiresonance designs. By matching multiple resonances of the plasmonic systems with the fundamental and generated nonlinear frequencies,[3,22−24] the nonlinear conversion efficiency can be boosted further. Recently, some groups have combined nanoantenna geometries and highly nonlinear materials, such as semiconductors, to achieve very efficient SHG.[25,26] However, near-field enhancement using the former two methods is still limited, mainly due to large damping losses from the metallic particles.

Received: May 17, 2018
Revised: August 1, 2018
Published: August 3, 2018

DOI: 10.1021/acs.nanolett.8b02005
Nano Lett. XXXX, XXX, XXX−XXX

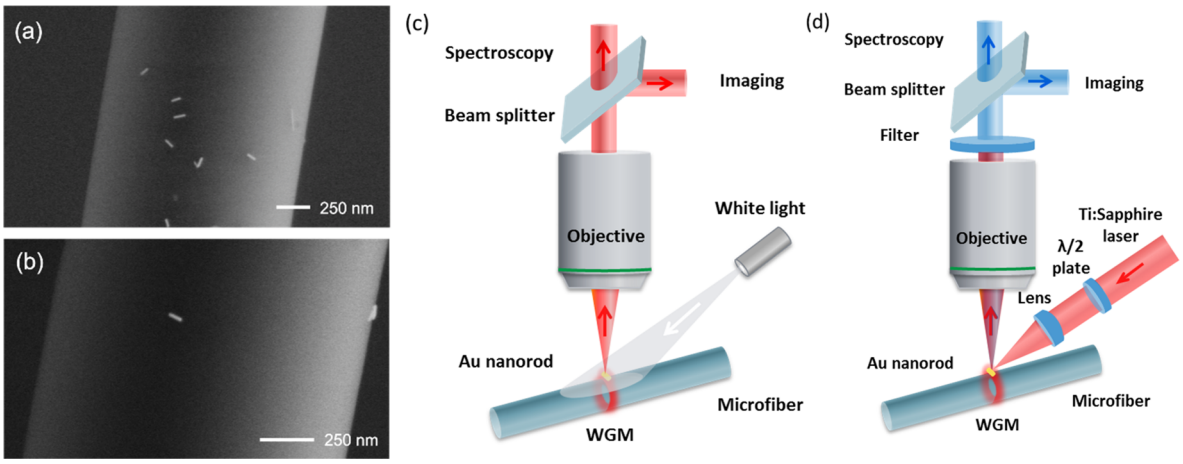

Figure 1. (a,b) SEM images of a silica microfiber with gold nanorods deposited on its surface. Schematic dark-field setup for (c) light scattering and (d) second-harmonic spectroscopy from single gold nanorods on tapered fibers.

On the theory side, an anharmonic oscillator model has been successfully exploited to provide instructive connections between linear and nonlinear properties of a plasmonic system[2−4,27] in which the linewidth $\Delta\omega$ of the linear resonance plays a key role in nonlinear yield. Intuitively, a narrow linewidth, which indicates a higher quality factor Q of the resonance, allows for light-matter interaction over a longer time period and also implies insignificant damping channels which bring benefit to strong near-field enhancement. The anharmonic oscillator model is able to predict a nonlinear signal that is superlinearly proportional to the inverse of the resonance linewidth[27,28] (e.g, for SHG, the nonlinear efficiency scales to $1/\Delta\omega^4$ if the plasmon resonance matches the fundamental frequency), which paves exciting avenues for highly efficient nonlinear optical processes at the nanoscale.

So far, different approaches have been used to decrease the line width of plasmonic resonances. One way is to tailor the aspect ratio toward very elongated rods.[29−31] Another way is to choose high-quality single-crystalline materials, which reduces damping by scattering at grain boundaries.[32] Still, the typical linewidths of single plasmonic rod antennas are around 50 nm.

Coupled systems with dark modes in plasmonic dimers,[33,34] trimers,[35] or oligomers[18,36] are capable to exhibit very sharp and narrow linewidths due to the inhibited radiative losses. In contrast to electromagnetically induced-transparency (EIT)-type coupling,[37] in which through destructive interference the transmission is enhanced and therefore weak light-matter interaction occurs, electromagnetically induced-absorption (EIA)- type coupling enables enhanced absorption of light by constructive interference of the coupled resonances in the materials. Previous attempts[2,38,39] achieved linewidths as small as several nanometers, and indeed succeeded in enhanced light-matter interaction for example in magneto-plasmonics.[40]

Different from those hybrid systems where only plasmonic modes are involved, here we demonstrate plasmonic nano-antennas coupled to silica microfibers,[41] resulting in ultra-narrow linear and nonlinear resonances. The silica fibers have been tapered to diameters below 2 μm and exhibit whispering gallery modes (WGMs) around their circumference. For a plasmon-fiber cavity, one of the WGMs couples efficiently to the longitudinal plasmon mode (at around 800 nm) of the adjacent gold nanoantenna that has been drop coated onto the surface of the fiber. When using side illumination with white light, an extremely narrow scattering peak [full width at half-maximum (FWHM) of typically 3 nm, corresponding to a quality factor up to 250] on top of a broad plasmonic resonance background can be observed. This means that the whispering gallery of the tapered microfiber acts as a high-Q resonator, causing the light to interact several hundred times in a coherent fashion with the gold nanorod. Such an enhanced coherent interaction leads to orders of magnitude increase of the nonlinear emission. We indeed observed a very high SHG yield using a femtosecond Ti:sapphire laser, up to 1000 times larger than for uncoupled gold nanoparticles. In addition, giant multiphoton photoluminescence takes place. Additional SHG spectroscopy was carried out, giving rise to an ultranarrow second-harmonic resonance (FWHM width of typically 6 nm if calculated at the fundamental wavelength) which can be well interpreted by a coupled anharmonic oscillator model.

For the experiment, single-crystalline gold nanorods were synthesized using an alternative seed-mediated method by exchanging the reducing agent with an excess of hydroquinone.[42,43] Compared with the conventional seed-mediated synthesis, high-purity nanorods with longitudinal surface plasmon resonances beyond 1000 nm could be grown. By modifying various parameters such as silver nitrate and seed concentration in the growth solution, we are able to control the aspect ratio of the gold nanorods over a wide range of the electromagnetic spectrum. The in this study employed gold nanorods exhibit plasmonic resonances in aqueous solution at around 950 nm [see the ultraviolet (UV)-visible (VIS) spectrum in Figure S1 of the Supporting Information]. A representative transmission electron microscope (TEM) image (upper inset of Figure S1) displays the high uniformity and narrow distribution of the nanoparticles. Their averaged aspect ratio is approximately 5. As the other element of the coupled systems, microfibers were manufactured by tapering single-mode fibers with a homemade flame-heated pulling machine[44] which enables precise tailoring of the diameter of the tapered fibers as well as their waist length. Microfibers with diameters in the range of 1.7−1.8 μm and a waist length of 2 cm were used to achieve the best coupling performances experimentally. The hybrid cavities were prepared by drop coating diluted gold solution onto the microfiber surface and waiting for several hours until it dried in ambient air. As an exemplary system, Figure 1a,b shows scanning electron microscopy images of a silica tapered fiber with gold nanorods placed on its surface. The gold nanorods are positioned randomly with different

DOI: 10.1021/acs.nanolett.8b02005
Nano Lett. XXXX, XXX, XXX−XXX

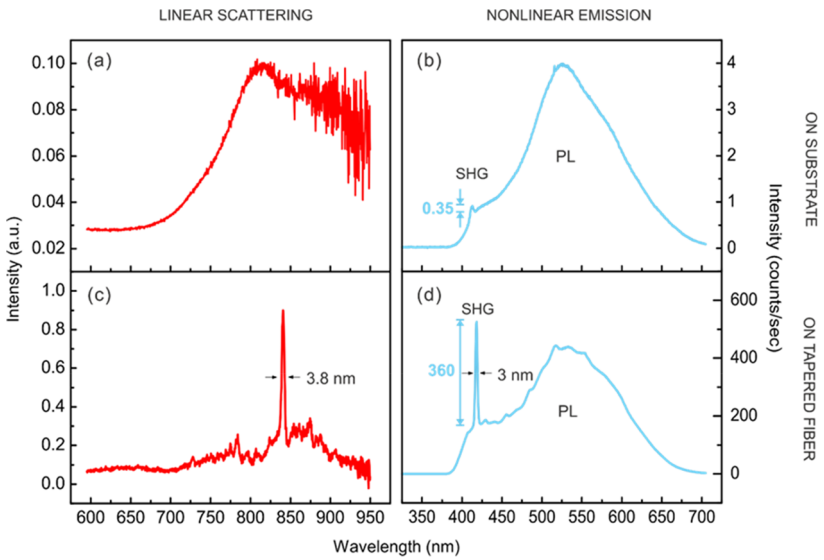

Figure 2. (a) Measured scattering and (b) nonlinear emission spectra of a single gold rod on a silica substrate surface. (c) Measured scattering and (d) nonlinear emission spectra of a single gold rod on a tapered fiber surface.

orientations, and the interparticle distance is usually large, so that strong dipole−dipole coupling between two gold nanorods does not take place.

The experimental setup for performing linear and nonlinear spectroscopy is schematically depicted in Figure 1c,d, respectively. To study the linear properties, an incoherent white-light source (Energetiq LDLS EQ-99) is utilized. The coupled systems are imaged and their scattering spectra are recorded based on a dark-field setup which includes a microscope combined with a grating spectrometer (Princeton Instruments IsoPlane 160) and a 2D CCD detector (Princeton Instruments PIXIS 256). It is worth noting that the incident angle with respect to the long axis of the fiber was chosen to be about 15 degrees in order to suppress the giant background scattering signal from the fiber surface efficiently. To investigate the nonlinear behavior of the hybrid cavities, a mode-locked Ti:sapphire oscillator is employed as the excitation light source (see Figure 1d). The laser delivers 100 fs optical pulses at 80 MHz repetition rate and allows wavelength tunability in the range of 760−850 nm. Due to the sensitive response of the coupled systems to the illumination configuration (see scattering spectra as a function of incident angle in detail in Figure S3), we shine the laser onto our samples at exactly the same incident angle as the white light, ascertained by a pair of diaphragms. Although we are currently not able to control the orientation of the gold nanorods on the fiber, efficient coupling between the plasmon longitudinal mode and the WGM can occur only if the gold nanorod does not lie in parallel to the fiber axis.

Therefore, we set the laser orthogonally polarized with respect to the fiber axis to excite the plasmon mode at about 800 nm. The laser is focused onto the samples via a lens with 25 mm focus length which leads to an elliptic beam spot of about 100 μm × 400 μm. An average power of about 600 mW is typically used, leading to a laser intensity of about 1.5 GW/cm^2 incident on our samples. This intensity is checked experimentally to be below the damage threshold of our hybrid cavities. Comparable peak intensities of the excitation laser were used in other nonlinear emission experiments of gold nanoparticles.[21,23,45] To filter out the intensely scattered fundamental light, a short-pass filter (FGB37) is added before the detector.

To demonstrate the extreme narrowing of the line width benefited from the efficient coupling between plasmon and whispering gallery modes, we compare the linear and nonlinear results from a single gold nanorod coupled to a silica tapered fiber with another uncoupled rod on a silica substrate. To ensure exactly the same experimental conditions (such as focus, illumination angle, and so forth) for both systems, we drop coat part of the gold nanorods solution right next to the microfiber onto the glass slide which held the fiber (diameter of about 1.80 μm). Figure 2a,c depicts the linear scattering spectra of the uncoupled and coupled systems, respectively. In stark contrast to the bare gold nanorod situation where scattering exhibits a FWHM of the spectrum on the order of 100 nm, the plasmon-fiber coupled configuration leads to a dramatic narrowing of the linewidth to 3.8 nm around 840 nm wavelength and simultaneously offers more than 10-fold enhancement in the peak scattering intensity. For the nonlinear characterization, the excitation laser wavelength is chosen to coincide with the spectral position where peak scattering occurs. Because of the unknown orientation of the individual gold nanorod, a half waveplate is used to adjust the state of polarization of the illumination light. By rotating the half waveplate and recording the nonlinear yield, we find the optimum irradiation condition for exciting the plasmon mode which led to maximum nonlinear light generation (see Figure 2b). The nonlinear spectrum of the isolated gold nanorod features a very weak SHG peak at about 420 nm together with a more pronounced and broader multiphoton photoluminescence background ranging from 400 nm beyond 700 nm. The SHG peak intensity on the top of the MPPL background is 0.35 counts per second, assuming incoherent superposition of SHG and MPPL spectra. In comparison, the coupled system yields much stronger nonlinear emission at the same excitation power (see Figure 2d). The sharp SHG peak possesses a FWHM width of about 3 nm and yields an SHG intensity of 360 counts per second, 3 orders of magnitude stronger than that from the isolated gold nanorod alone in Figure 2b. In addition, the plasmon-fiber coupling contributes to 2 orders of

DOI: 10.1021/acs.nanolett.8b02005
Nano Lett. XXXX, XXX, XXX−XXX

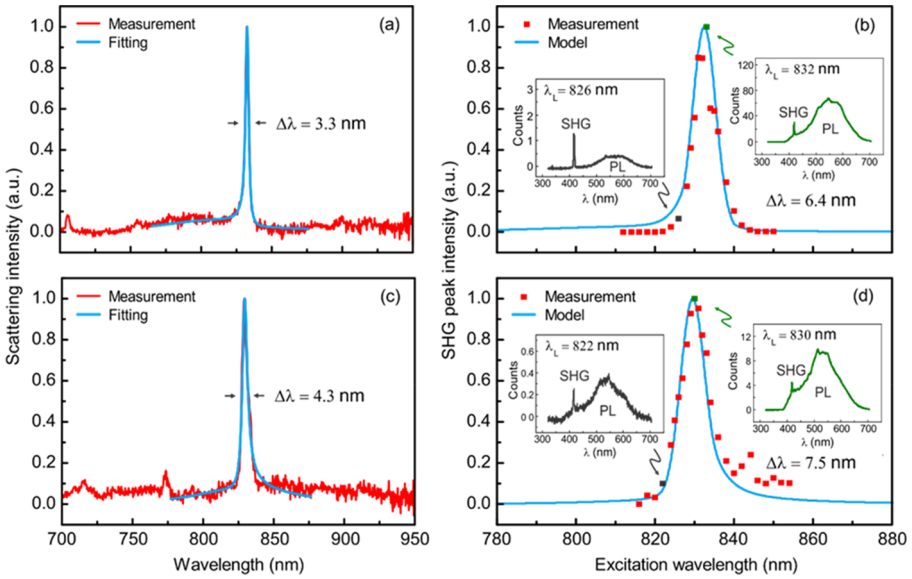

Figure 3. Measured and modeled linear and nonlinear responses. (a,c) Scattering spectra (red, measurement; blue, fit) from two gold rods coupled to similar microfibers with a diameter of about 1.8 μm, while (b,d) are their corresponding SHG efficiency as a function of excitation laser wavelength (red dots, measurement; blue curves, model). In (b,d), nonlinear emission spectra at several typical excitation wavelengths (λ_L) are shown in the insets (black and green curves). The FWHM linewidths $\Delta\lambda$ of the linear and the second-harmonic resonances are marked in (a–d).

magnitude enhancement of the MPPL yield as well. It is interesting to see that the broad MPPL spectrum is regularly modulated by several whispering gallery modes located in the corresponding spectral window, which causes slight fringes while absent in the isolated gold nanorod situation. In both systems, the peaks of the MPPL spectra, which are located at around 520 nm, are dominated mainly by the band structure of gold. The entire profile of MPPL is determined by the gold nanoparticle[14] and our experimental setup, for instance, the short-pass filter before our detector. According to the similar nonlinear emission profiles from both uncoupled and coupled systems, we believe that it is gold which acts as our efficient nonlinear source for frequency up-conversion. Also, it is worth noting that the 1000-fold enhancement of SHG scattering is a moderate value, because some uncoupled gold nanorods produced nearly undetectable SHG signals.

In order to study the wavelength-dependent SHG efficiency and characterize the second-harmonic resonances, we tune the center wavelength of our excitation laser over the linear resonances step by step. For better comparison, we choose two hybrid cavities which exhibit different linewidths as well as distinct resonance wavelengths. Figure 3a,c shows the linear scattering spectra (red curves, normalized to [0,1]) from two gold nanorods coated onto the surface of tapered fibers with diameters around 1.78 and 1.80 μm, respectively. The FWHM $\Delta\lambda$ of the single-band scattering is equal to 3.3 and 4.3 nm, which corresponds to a high Q factor $\lambda/\Delta\lambda$ of 250 and 190, respectively. The resonances λ are located at 832.3 and 829.2 nm. Here, more efficient coupling between plasmon and WGMs causes a higher signal-to-noise ratio, and hence several tiny peaks arising from other WGMs are easily visible in the background, as opposed to Figure 2c. By sweeping the laser wavelength, we get a series of nonlinear emission spectra in which SHG and MPPL features are both observable (see the insets in Figure 3b,d for exemplary results, all normalized to the same incident power and exposure time). Similar to Figure 2d, the linewidth of the SHG peak is again roughly 3 nm, although a slight dependence on the excitation wavelength is present which ranges between half the linear resonance linewidth and half the laser spectral width. The SHG peak position is also determined by the interplay between linear properties of the system and the excitation laser (see Figure S4 of Supporting Information). For every spectrum, we analyze the SHG peak intensity by subtracting the MPPL baseline and then dividing it by the product of laser power squared and exposure time. After plotting it as a function of excitation wavelength, the nonlinear spectroscopy gives rise to ultra-narrow second-harmonic resonances of the two coupled systems, as depicted by the red squares in Figure 3b,d (normalized again to [0,1], for convenient comparison with our model shown later). The linewidths of the nonlinear resonances are 6.4 and 7.5 nm respectively if calculated at the fundamental wavelength, which lies between the value for the width of the linear resonance and our excitation laser linewidth (about 9 nm). Furthermore, it is apparent that the maximum SHG efficiency occurs almost at the wavelength of the linear resonance.

In order to analyze the relationship between the linear and nonlinear optical responses from these hybrid cavities, we employ a coupled anharmonic oscillator model in which the plasmon mode (P subscript) and the WGM (W subscript) are treated as two classical oscillators. The equations of motion considering a small perturbation as the origin of SHG read then

$$\ddot{x}_P + 2\gamma_P\dot{x}_P + \omega_P^2 x_P - \kappa x_W + a_P x_P^2 = -\frac{e}{m}E(t) \quad (1)$$

$$\ddot{x}_W + 2\gamma_W\dot{x}_W + \omega_W^2 x_W - \kappa x_P + a_W x_W^2 = 0 \quad (2)$$

where x_j denotes the displacement, γ_j represents the damping constant that is proportional to the linewidth of the mode, ω_j corresponds to the resonance frequency of an unperturbed oscillator, κ is the coupling constant addressing energy interchange between these two modes, and a_j describes the SHG strength (j = P or W). e and m are the charge and the mass of the oscillator corresponding to the plasmon mode.

DOI: 10.1021/acs.nanolett.8b02005
Nano Lett. XXXX, XXX, XXX−XXX

Solving the equations in the unperturbed situation by means of Fourier transform leads to scattering which is proportional to $\left|\frac{g_P}{1-\kappa^2 g_P g_W}\right|^2$, where the linear response function $g_j = \frac{1}{\omega_j^2 - \omega^2 - 2i\gamma_j\omega}$ (j = P or W). By fitting our measured scattering spectra of the hybrid systems with this expression, the constant parameters γ_j, ω_j, and κ can be extracted. The blue curves in Figure 3a,c depict the excellent fitting results, which reflects the good applicability of our model here. In particular, it is able to reproduce the asymmetrical profiles of the scattering spectra on the edge (see more results in Figure S2) which stem from Fano-like coupling between plasmon and WGMs.

On the basis of the ansatz $x_P(t) = x_P^{(1)}(t) + a_P x_P^{(2)}(t)$, the second correction term oscillating at the SHG frequency is described by $x_P^{(2)}(2\omega) \propto \mathrm{FT}\{[\,x_P^{(1)}(t)]^2\}$ in frequency domain, where FT denotes Fourier transform. Here, we neglect the linear response function g_P at the SHG frequency because it is spectrally flat and small for our gold nanorods which show no resonance at the harmonic frequency. In addition, we assume that the nonlinear emission we observe experimentally mainly stems from the single gold nanorod, rather than from the microfiber. On the one hand, linear simulation enables the prediction of a much higher near-field in the vicinity of the gold nanorod than along the microfiber.[41] On the other hand, gold is considered a highly nonlinear material in general, whereas fused silica possesses vanishing second-order susceptibilities owing to inversion symmetry. Even if the microscopic symmetry is broken, for instance, by placing the gold rod on the surface, the nonlinearity from fused silica should still be very weak. One indirect proof is that one observes highly efficient MPPL mainly related to the band structure of gold in all of our nonlinear emission spectra). Indeed, this assumption works quite well, as one can see from the excellent agreement between the SHG measurement and the results predicted by our nonlinear oscillator model (denoted by blue curves).

Note that in our model we use an ultrashort optical pulse with FWHM of 100 fs in accordance with the experimental laser source. This way, the second-harmonic resonances show broader linewidths than the linear counterparts, because they involve convolution effects arising from the broader spectral width of the excitation laser. Therefore, the linewidths of our SHG resonances are limited by our laser source at this moment. Our model suggests that it is possible to achieve a nonlinear resonance as narrow as that in the linear regime as long as the excitation laser exhibits a narrower optical spectrum than the resonance itself (all considered at fundamental wavelength). The nonlinear oscillator model is also able to predict the much higher nonlinear conversion efficiency from the coupled cavity with higher Q factor in Figure 3a when compared to that with the lower Q factor in Figure 3c. Indeed, as shown by the insets of Figure 3b,d, the hybrid plasmon-fiber cavity with narrower linewidth and higher Q factor enables stronger nonlinear emission experimentally. It confirms once more the advantage of our coupling system which leads to less radiative losses.

When we compare the SHG peak and MPPL peak carefully in all the insets of Figure 3b,d, it is interesting to see that the intensity ratio between them is sensitive to the excitation wavelength. It implies that the two nonlinear optical processes might originate from different nonlinear orders. To fully determine the two nonlinear processes, we measure a series of nonlinear emission spectra as a function of excitation laser power from 330 to 600 mW for a typical coupled system. The incident laser is fixed at 828 nm which matches the resonance of the plasmon-fiber cavity. By assuming again incoherent interplay between SHG and MPPL, we are able to plot SHG peak intensity and MPPL integrated intensity (area of the MPPL envelope from 380 to 700 nm) in dependence of the excitation power. The results are plotted in Figure 4a on double logarithmic scale (red squares and open circles, respectively). The measurement results are then fitted by a linear function, where the fitted slope represents the nonlinear order. The red and black solid curves exhibit excellent fitting for SHG and MPPL, where the SHG process is confirmed by the slope of 2, while MPPL seems to involve cascaded absorption of higher photon numbers (slope of nearly 5). In order to gain more insight on the MPPL process, we evaluate

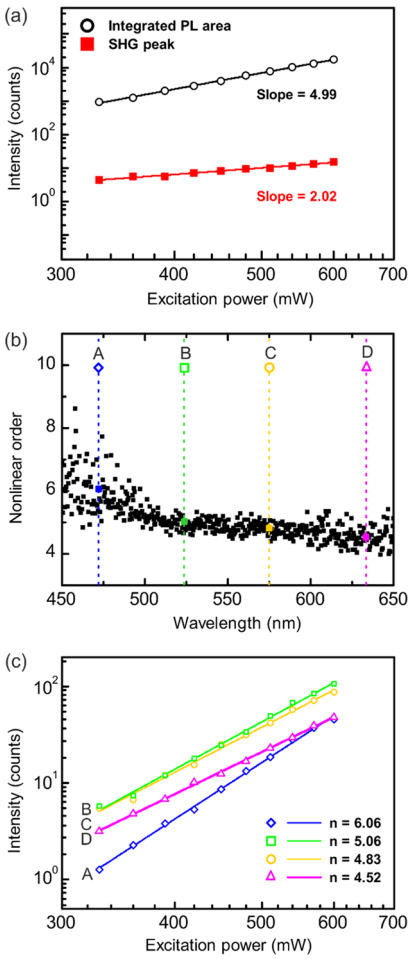

Figure 4. Power dependence of the nonlinear emission obtained from a gold nanorod on a tapered fiber. (a) Peak intensity of SHG and integrated intensity of multiphoton photoluminescence in dependence on excitation power. Excellent linear fitting at log–log scale shows anticipated power-law of the nonlinear responses. (b) Nonlinear order of MPPL as a function of emission wavelength. The vertical lines (A, B, C, and D) mark spectral positions where the measurements and fits of the power dependence are shown in (c). The experimental data points in (c) are denoted by symbols, while the solid lines in this double-logarithmic graph show the linear fits determining the nonlinear order plotted in (b).

DOI: 10.1021/acs.nanolett.8b02005
Nano Lett. XXXX, XXX, XXX−XXX

the MPPL intensity at each emission wavelength as a function of the laser power so that a spectrally resolved analysis of the excitation power dependence can be achieved (see Figure 4b). Despite increasing fitting error on both edges (near 450 and 650 nm) due to the limitation of our setup, the nonlinear order shows a clear trend of monotonic decrease toward longer emission wavelength. The slope changes from roughly 6.1 to 4.5 from 450 to 650 nm, leading to an average nonlinear order of about 5. To demonstrate our reliable fitting, data points at four selected emission wavelengths are given in Figure 4c in detail (marked by A, B, C, and D), where excellent linear fitting is confirmed by solid curves. Similar phenomena of high-nonlinear-order MPPL sensitive to emission wavelength have recently been reported by Knittel et al.[15] A hot electron bath out of equilibrium can be created when the material interacts with intense ultrashort pulses and hence the exponential tail of the Fermi−Dirac distribution generates the high-energy photoluminescence with an effectively higher nonlinear order.[13,15] Additionally, it has been found that the MPPL order is sensitively dependent on the pump laser properties as well.[16,46] Its spectral shape is related to the geometry and crystallinity of the gold nanoparticles.[13,47,48] In our hybrid systems, the MPPL yield can be similarly high or even much stronger compared to SHG scattering, when the excitation laser hits the resonance perfectly (also see the insets of Figure 3b,d). Such an efficient MPPL emission with nonlinear order up to 6 is very rare in single gold nanoparticle systems reported so far and might also benefit from the large nonlinearities of our hybrid cavities.

In conclusion, we have successfully realized ultranarrow second-harmonic resonances with linewidth down to 7 nm based on hybrid plasmon-fiber cavities. The efficient coupling between plasmon modes and WGMs reconfigures trapped light around the hybrid systems which leads to less radiative losses and therefore boosted optical near-fields in comparison to isolated gold nanorods. This way the second-harmonic conversion efficiency of our hybrid cavities can be typically 1000-fold larger than that of a gold nanorod on a silica substrate. Additionally, a coupled anharmonic oscillator model describes the wavelength-dependent second-harmonic efficiencies very well. Gaining from the high quality factor Q of the coupled system, efficient multiphoton photoluminescence processes with a nonlinear order up to 6 have been experimentally observed as well. Our work takes the advantages of both plasmonic near-field enhancement and light trapping capability of WGMs, which could allow for ultrasensitive nonlinear sensing, extremely efficient nonlinear frequency conversion, and broadband incoherent local light sources at the nanoscale.

■ ASSOCIATED CONTENT

Supporting Information

The Supporting Information is available free of charge on the ACS Publications website at DOI: 10.1021/acs.nanolett.8b02005.

Characterization of the high-quality gold nanorods we used in the work; spectral tunability of hybrid resonance; linear scattering spectra of the hybrid plasmon-fiber cavities sensitive to incident angle; scattered laser spectra and second-harmonic emission spectra dependent on different excitation laser wavelengths; fitting parameters of linear scattering of hybrid systems (PDF)

■ AUTHOR INFORMATION

Corresponding Authors

*E-mail: q.ai@pi4.uni-stuttgart.de.
*E-mail: l.gui@pi4.uni-stuttgart.de.
*E-mail: h.giessen@pi4.uni-stuttgart.de.

ORCID

Qi Ai: 0000-0002-1716-7638
Lili Gui: 0000-0002-3710-6330
Ksenia Weber: 0000-0002-9836-8457

Notes

The authors declare no competing financial interest.

■ ACKNOWLEDGMENTS

The authors gratefully acknowledge financial support from DFG (SPP 1391), BW-Stiftung, Carl-Zeiss Stiftung, China Scholarship Council (CSC), ERC (ComplexPlas). The authors thank Sirin Celiksoy for synthesizing gold nanorods in an early stage of the experiment. Also, we would like to thank Nikolai Strohfeldt and Florian Sterl for their valuable technical support.

■ REFERENCES

(1) Ko, K. D.; Kumar, A.; Fung, K. H.; Ambekar, R.; Liu, G. L.; Fang, N. X.; Toussaint, K. C. *Nano Lett.* **2011**, *11*, 61−65.
(2) Metzger, B.; Schumacher, T.; Hentschel, M.; Lippitz, M.; Giessen, H. *ACS Photonics* **2014**, *1*, 471−476.
(3) Metzger, B.; Gui, L.; Fuchs, J.; Floess, D.; Hentschel, M.; Giessen, H. *Nano Lett.* **2015**, *15*, 3917−3922.
(4) Gui, L.; Bagheri, S.; Strohfeldt, N.; Hentschel, M.; Zgrabik, C. M.; Metzger, B.; Linnenbank, H.; Hu, E. L.; Giessen, H. *Nano Lett.* **2016**, *16*, 5708−5713.
(5) Accanto, N.; Piatkowski, L.; Hancu, I. M.; Renger, J.; Van Hulst, N. F. *Appl. Phys. Lett.* **2016**, *108*, 083115.
(6) Linnenbank, H.; Linden, S. *Optica* **2015**, *2*, 698−701.
(7) Raschke, M. B.; Berweger, S.; Atkin, J. M. *Plasmonics: Theory and Applications*; Springer: Dodrecht, 2013; pp 237−281.
(8) Renger, J.; Quidant, R.; Van Hulst, N.; Palomba, S.; Novotny, L. *Phys. Rev. Lett.* **2009**, *103*, 1−4.
(9) Kravtsov, V.; Ulbricht, R.; Atkin, J. M.; Raschke, M. B. *Nat. Nanotechnol.* **2016**, *11*, 459−464.
(10) Vasa, P.; Wang, W.; Pomraenke, R.; Lammers, M.; Maiuri, M.; Manzoni, C.; Cerullo, G.; Lienau, C. *Nat. Photonics* **2013**, *7*, 128−132.
(11) Yi, J.; Groß, P.; Lienau, C. *World Scientific Handbook of Metamaterials and Plasmonics*; World Scientific, 2017; pp 255−306.
(12) Castro-Lopez, M.; Brinks, D.; Sapienza, R.; Van Hulst, N. F. *Nano Lett.* **2011**, *11*, 4674−4678.
(13) Wang, S.; Xi, W.; Cai, F.; Zhao, X.; Xu, Z.; Qian, J.; He, S. *Theranostics* **2015**, *5*, 251−266.
(14) Knittel, V.; Fischer, M. P.; De Roo, T.; Mecking, S.; Leitenstorfer, A.; Brida, D. *ACS Nano* **2015**, *9*, 894−900.
(15) Knittel, V.; Fischer, M. P.; Vennekel, M.; Rybka, T.; Leitenstorfer, A.; Brida, D. *Phys. Rev. B: Condens. Matter Mater. Phys.* **2017**, *96*, 1−6.
(16) Biagioni, P.; Brida, D.; Huang, J. S.; Kern, J.; Duò, L.; Hecht, B.; Finazzi, M.; Cerullo, G. *Nano Lett.* **2012**, *12*, 2941−2947.
(17) Lee, J.; Tymchenko, M.; Argyropoulos, C.; Chen, P. Y.; Lu, F.; Demmerle, F.; Boehm, G.; Amann, M. C.; Alù, A.; Belkin, M. A. *Nature* **2014**, *511*, 65−69.
(18) Grinblat, G.; Rahmani, M.; Cortés, E.; Caldarola, M.; Comedi, D.; Maier, S. A.; Bragas, A. V. *Nano Lett.* **2014**, *14*, 6660−6665.
(19) Chen, K.; Durak, C.; Heflin, J. R.; Robinson, H. D. *Nano Lett.* **2007**, *7*, 254−258.
(20) Albrecht, G.; Hentschel, M.; Kaiser, S.; Giessen, H. *ACS Omega* **2017**, *2*, 2577−2582.
(21) Pu, Y.; Grange, R.; Hsieh, C. L.; Psaltis, D. *Phys. Rev. Lett.* **2010**, *104*, 1−4.

DOI: 10.1021/acs.nanolett.8b02005
Nano Lett. XXXX, XXX, XXX−XXX

(22) Linnenbank, H.; Grynko, Y.; Förstner, J.; Linden, S. *Light: Sci. Appl.* **2016**, *5*, e16013.
(23) Celebrano, M.; Wu, X.; Baselli, M.; Großmann, S.; Biagioni, P.; Locatelli, A.; De Angelis, C.; Cerullo, G.; Osellame, R.; Hecht, B.; Duò, L.; Ciccacci, F.; Finazzi, M. *Nat. Nanotechnol.* **2015**, *10*, 412−417.
(24) Thyagarajan, K.; Rivier, S.; Lovera, A.; Martin, O. J. F. *Opt. Express* **2012**, *20*, 12860.
(25) Ghirardini, L.; Carletti, L.; Gili, V.; Pellegrini, G.; Duò, L.; Finazzi, M.; Rocco, D.; Locatelli, A.; De Angelis, C.; Favero, I.; Ravaro, M.; Leo, G.; Lemaître, A.; Celebrano, M. *Opt. Lett.* **2017**, *42*, 559.
(26) Vabishchevich, P. P.; Liu, S.; Sinclair, M. B.; Keeler, G. A.; Peake, G. M.; Brener, I. *ACS Photonics* **2018**, *5*, 1685−1690.
(27) Hentschel, M.; Utikal, T.; Giessen, H.; Lippitz, M. *Nano Lett.* **2012**, *12*, 3778−3782.
(28) Metzger, B.; Hentschel, M.; Lippitz, M.; Giessen, H. *Opt. Lett.* **2012**, *37*, 4741.
(29) Sönnichsen, C.; Franzl, T.; Wilk, T.; von Plessen, G.; Feldmann, J.; Wilson, O.; Mulvaney, P. *Phys. Rev. Lett.* **2002**, *88*, 774021−774024.
(30) Ye, X.; Gao, Y.; Chen, J.; Reifsnyder, D. C.; Zheng, C.; Murray, C. B. *Nano Lett.* **2013**, *13*, 2163−2171.
(31) Mayer, M.; Scarabelli, L.; March, K.; Altantzis, T.; Tebbe, M.; Kociak, M.; Bals, S.; Garciá De Abajo, F. J.; Fery, A.; Liz-Marzán, L. M. *Nano Lett.* **2015**, *15*, 5427−5437.
(32) Huang, J. S.; Callegari, V.; Geisler, P.; Brüning, C.; Kern, J.; Prangsma, J. C.; Wu, X.; Feichtner, T.; Ziegler, J.; Weinmann, P.; Kamp, M.; Forchel, A.; Biagioni, P.; Sennhauser, U.; Hecht, B. *Nat. Commun.* **2010**, *1*, 150−158.
(33) Bachelier, G.; Russier-Antoine, I.; Benichou, E.; Jonin, C.; Del Fatti, N.; Vallée, F.; Brevet, P. F. *Phys. Rev. Lett.* **2008**, *101*, 5−8.
(34) Aouani, H.; Rahmani, M.; Navarro-Cía, M.; Maier, S. A. *Nat. Nanotechnol.* **2014**, *9*, 290−294.
(35) Alegret, J.; Rindzevicius, T.; Pakizeh, T.; Alaverdyan, Y.; Gunnarsson, L.; Käll, M. *J. Phys. Chem. C* **2008**, *112*, 14313−14317.
(36) Rahmani, M.; Lei, D. Y.; Giannini, V.; Lukiyanchuk, B.; Ranjbar, M.; Liew, T. Y. F.; Hong, M.; Maier, S. A. *Nano Lett.* **2012**, *12*, 2101−2106.
(37) Liu, N.; Langguth, L.; Weiss, T.; Kästel, J.; Fleischhauer, M.; Pfau, T.; Giessen, H. *Nat. Mater.* **2009**, *8*, 758−762.
(38) Taubert, R.; Hentschel, M.; Kästel, J.; Giessen, H. *Nano Lett.* **2012**, *12*, 1367−1371.
(39) Taubert, R.; Hentschel, M.; Giessen, H. *J. Opt. Soc. Am. B* **2013**, *30*, 3123.
(40) Floess, D.; Hentschel, M.; Weiss, T.; Habermeier, H. U.; Jiao, J.; Tikhodeev, S. G.; Giessen, H. *Phys. Rev. X* **2017**, *7*, 1−10.
(41) Wang, P.; Wang, Y.; Yang, Z.; Guo, X.; Lin, X.; Yu, X. C.; Xiao, Y. F.; Fang, W.; Zhang, L.; Lu, G.; Gong, Q.; Tong, L. *Nano Lett.* **2015**, *15*, 7581−7586.
(42) Vigderman, L.; Zubarev, E. R. *Chem. Mater.* **2013**, *25*, 1450−1457.
(43) Schnepf, M. J.; Mayer, M.; Kuttner, C.; Tebbe, M.; Wolf, D.; Dulle, M.; Altantzis, T.; Formanek, P.; Förster, S.; Bals, S.; König, T. A. F.; Fery, A. *Nanoscale* **2017**, *9*, 9376−9385.
(44) Pricking, S.; Giessen, H. *Opt. Express* **2010**, *18*, 3426−3437.
(45) Genevet, P.; Tetienne, J. P.; Gatzogiannis, E.; Blanchard, R.; Kats, M. A.; Scully, M. O.; Capasso, F. *Nano Lett.* **2010**, *10*, 4880−4883.
(46) Muhlschlegel, P.; Eisler, H. J.; Martin, O. J.; Hecht, B.; Pohl, D. W. *Science (Washington, DC, U. S.)* **2005**, *308*, 1607−1609.
(47) Wang, D.-S.; Hsu, F.-Y.; Lin, C.-W. *Opt. Express* **2009**, *17*, 11350.
(48) Lippitz, M.; Van Dijk, M. A.; Orrit, M. *Nano Lett.* **2005**, *5*, 799−802.

DOI: 10.1021/acs.nanolett.8b02005
Nano Lett. XXXX, XXX, XXX−XXX